Extreme Mechanics Letters 15 (2017) 51–56

Contents lists available at ScienceDirect

Extreme Mechanics Letters

journal homepage: www.elsevier.com/locate/eml

Buckling shape transition of an embedded thin elastic rod after failure of surrounding elastic medium

Amir Mohammadi Nasab [a], Dong Wang [b], Zi Chen [b], Wanliang Shan [a,*]

[a] Department of Mechanical Engineering, University of Nevada, Reno, NV 89557, USA
[b] Thayer School of Engineering, Dartmouth College, Hanover, NH 03755, USA

ARTICLE INFO

Article history:
Received 14 February 2017
Received in revised form 25 April 2017
Accepted 31 May 2017

Keywords:
Short wavelength buckling
Elastic medium
Fracture
Genetic algorithm

ABSTRACT

When the compressive load to a thin elastic rod embedded in an elastic medium exceeds a threshold, the thin rod buckles into an exponentially decaying short wavelength profile to minimize the total energy of the system. As the compressive load continues to increase, the buckling amplitude increases correspondingly, until the rod/medium interface fractures and the short wavelength buckling profile morphs into a different shape as fracture propagates into the surrounding medium. In this study, such shape transition in the presence of surrounding medium failure is investigated using a combined experimental and theoretical approach. We identify the ansatz that can be used to describe the post-fracture buckling profile, and then develop a forward scheme using the energy principle to predict the buckling profile of the thin rod when fracture happens in the medium. We also develop a backward scheme where we use the post-fracture buckling profile to estimate the buckling profile before fracture of the surrounding medium. Comparison of experimental and theoretical results indicates that the modeling framework can be used to characterize the buckling profile transition of a thin elastic rod embedded in a fractured elastic medium.

1. Introduction

Traditionally, buckling of thin rods has been mostly considered as a failure mechanism to be avoided in engineering design. Recently, however, it has gradually been revealed that, as a form of mechanical instability, buckling plays a key role in the morphology generation of many natural systems [1–17]. Examples include the morphology of plant roots [1,2], oil pipes [3–5], elastic and viscoelastic films and shells [6–8], cytoskeletal microtubules in living cells [9–12], thin rods embedded in matrix [13–15] or granular media [16], and tortuous arteries [17]. For engineering structures, buckling and post-buckling behavior of infinite beams on nonlinear elastic foundations has also been studied using Koiter's improved theory [18]. Thus buckling phenomena have been investigated extensively to understand the fundamental mechanics, as well as to design synthetic systems taking advantage of this mechanical instability.

A thin elastic rod under axial compression tends to deform into a shape corresponding to its lowest deformation energy state. At low axial compressive forces, the rod experiences pure axial compression. Exceeding a critical compression threshold, the rod buckles with a certain mode number n that depends on the bending rigidity of the rod and the elastic properties of the medium where the thin rod is placed. In media with negligible elastic modulus such as air, the rod tends to buckle with the longest possible wavelength, which is on the same order as the rod length, with a pre-factor depending on the boundary conditions. However, when embedded in an elastic medium with a finite elastic modulus, the buckling wavelength decreases and the critical buckling force threshold increases [9]. Specifically, this short wavelength buckling mechanism may hold the key to understanding how microtubules can strengthen the structure of living cells [9–12].

As observed experimentally, there is a decay length in the buckling profile of microtubules within cells when the microtubules interact with cell periphery [9]. Das et al. predicted a decay length of buckling profile of a thin elastic rod embedded in an elastic medium with nonlinear elastic behavior [10]. Shan et al. modeled buckling of a superelastic rod in a biopolymer matrix using a similar theoretical framework, and showed experimentally that the nonlinear elastic behavior of the medium is outweighed by the linear responses, as predicted by modeling results [13]. To our best knowledge, however, all previous works have only investigated the buckling phenomenon assuming small deformations in the surrounding media, excluding the possibility of any failure of the embedding medium. For a thin elastic rod embedded in a biopolymeric matrix, as the amplitude of the short wavelength buckling increases, the deformation of the surrounding media in the vicinity

* Corresponding author.
E-mail address: wshan@unr.edu (W. Shan).

http://dx.doi.org/10.1016/j.eml.2017.05.006
2352-4316/

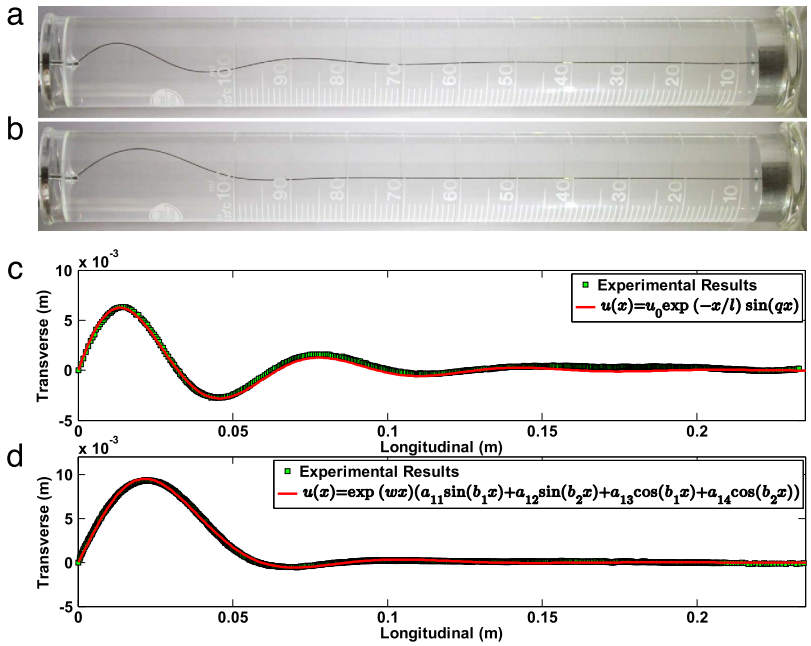

Fig. 1. (a) Buckling shape of a compressed wire embedded in gelatin before fracture. (b) Buckling shape of a compressed wire embedded in gelatin after fracture. (c) The deformation profile of the compressed wire in panel (a) and a fitted curve by Matlab. (d) The deformation profile of the compressed wire in panel (b) and a fitted curve by Matlab.

of the rod also increases. At certain point, the distinct interface between the rod and the polymeric medium will fail. Then the crack will propagate into the elastic medium and finally stops at a position that a new balance is reached (Fig. 1). This failure behavior may not happen in nature such as microtubules buckling during interaction with cell periphery, since the cytoplasm in living cells is more viscoelastic than gelatin, but it is critical to understand the mechanical behavior of engineered biomimetic systems where fracture in the medium can occur.

In this paper, we show experimentally the shape transition of the buckling profile of a biopolymer-reinforced rod when the surrounding matrix fractures. We identify a model that can be used to describe the post-fracture buckling profile. We then present both forward and backward schemes to predict the short wavelength buckling shape transition. For forward buckling shape transition, we treat the buckling profile as a 2D crack front and use crack propagation criteria to determine the buckling profile of the rod after failure of the medium, taking the buckling profile right before fracture as input. For the backward scheme, our method balances the deformation energy of the rod and the medium before and after the failure of the matrix to estimate the short wavelength buckling profile before fracture, taking the post-fracture profile as input. We also conduct a series of experiments featuring surrounding media with different elastic moduli to verify the applicability of our modeling framework. By providing new knowledge of the fundamental mechanics, these results will help understand buckling of microtubules in single cells, and shed light on new design principles for biologically inspired materials.

2. Materials and methods

2.1. Experiments

To experimentally investigate the buckling profile of a thin elastic rod in a biopolymer matrix, we use superelastic nitinol wires (55% nickel, 45% titanium) with a diameter of 203.2 μm obtained from Small Parts, Inc., which were straightened and annealed by the manufacturer per ASTM F2063. We assessed the Young's modulus, E, of the wires at room temperature to be $E = 60.8 \pm 1.0$ GPa [13]. We use porcine gelatin (Sigma Aldrich) with a Bloom value of 300 and concentrations of 20 g/l, 25 g/l and 30 g/l for the embedding matrix. Bloom value is a standard industrial measure to assess gelatin quality and is associated with the shear modulus of gelatin gels. Shear moduli of gelatin media used in this study were estimated to be $G = 0.64$ kPa, $G = 0.87$ kPa and $G = 1.12$ kPa for concentrations of 20 g/l, 25 g/l and 30 g/l, respectively [13,19]. We inserted nitinol wires with a length of 22.5 cm into graduated cylinders filled with liquid gelatin solutions. Then we put the samples in a fridge at a temperature of 5 °C for 24 h. After that the gelatin solution solidified and the nitinol wire was embedded inside biopolymer matrices, aligned along the axis of the graduated cylinder. The samples were exposed to room temperature at 24 °C for 5 h before testing.

The compressive force was exerted from one end of the wire using an adapter to simulate the hinged boundary condition while the other end of the wire was hinged with another adapter that was placed at the bottom of the graduated cylinder (Fig. 2). We increased the compressive loading quasi-statically using an ElectroForce® 3330 test instrument until we got close to the critical values for failure observed previously by Shan et al. [13]. We then increased the displacement step by step with a step size of 0.2 mm and a constant displacement rate of 0.1 mm/s within each step. We did this because it is well known that delayed fracture is common for soft and brittle gels [20]. Between the steps we held the displacement still for 10 s to observe whether failure occurred or not. If not, we further increased the loading until the abrupt shape transition was observed. Digital images of the rod deflections before and after the gelatin failure were taken by a Canon HD digital camera (EOS Rebel T5i). An image analysis code written in Matlab was used to analyze the images of rod deflections.

2.2. Theory and modeling

It has been reported in the previous studies [10,13] and also observed in the current work that the rod buckles in a plane and does not show any out-of-plane rotations for both of the pre- and post-fracture cases, provided that the rod in the graduated cylinder is aligned approximately in an axisymmetric manner. The

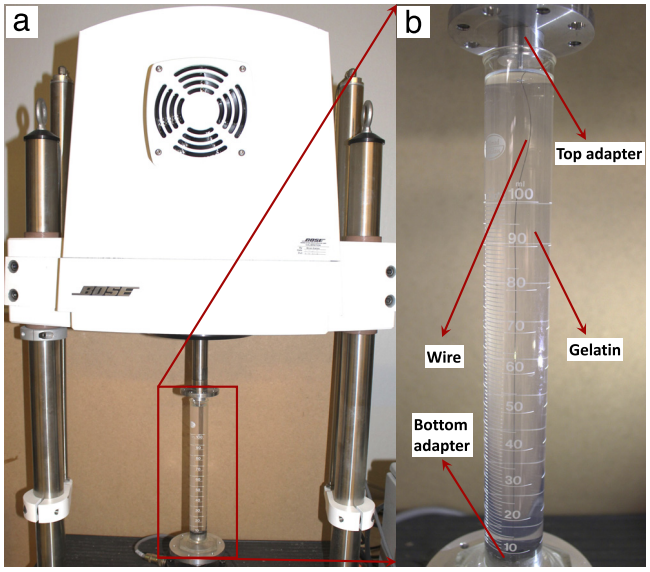

Fig. 2. (a) Image of the experimental setup under the ElectroForce® 3330 test instrument. (b) Image of the experimental setup showing the adapters and the embedded thin wire under the testing instrument.

2D transverse displacement of a buckled rod before failure of the surrounding medium can be described by [10]:

$$u_1(x) = u_0 \exp\left(\frac{-x}{l}\right) \sin(qx), \tag{1}$$

where x is the distance from the free end of the rod where compressive loading is applied, l is the decay length, and q is related to the buckling wavelength λ through $q = 2\pi/\lambda$. Also consistent with previous studies, the energy function Π of the rod and the medium for small deformations of the rod neglecting the nonlinear properties of the medium is as follows:

$$\Pi = -fv(0) + \int_0^\infty dx \left[\frac{\kappa}{2}u''^2(x) + \frac{1}{2}\alpha_\perp u^2(x) + \frac{1}{2}\alpha_\parallel v^2(x)\right], \tag{2}$$

where f is the compressive force exerted on the rod at $x = 0$ and $v(x) = \int_x^\infty ds[u'(s)^2/2]$ is the longitudinal displacement of an inextensible rod [13]. $\alpha_\perp$ and $\alpha_\parallel$ are the elastic coupling parameters governed by the dimensions of the rod and the elasticity of the medium. For a straight rod of a diameter d with perfect coupling to an elastic medium: $\alpha_\perp = 4\pi G/ln(2\lambda/d)$ and $\alpha_\parallel = \alpha_\perp/2$, where G is the shear modulus of the matrix[13]. It has also been shown in Ref. [13] that the exponentially decaying behavior of the buckling profile can be quantitatively accounted for using a model that considers no-slip coupling between the wire and the medium within a linear framework.

When the amplitude of the short wavelength buckling increases with loading and eventually the maximum strain exceeds some critical value, however, interfacial fracture will initiate in the vicinity of the region where the highest transverse displacement is located. The failure might further develop along the interface and also into the surrounding medium until the whole structure reaches another minima of its total potential energy. In the end, the surrounding medium are broken into two regions, one fractured and the other not fractured, with the fractured region close to the loading end of the rod. Clearly, in the fractured region the elastic deformation of the surrounding medium is much reduced during the crack propagation process. If the medium is brittle, this elastic energy should be negligible.

Inspired by a recent work on reinforced rod buckling in two distinct media by Wang et al. [21], we hereby assume that after fracture the transverse displacement of the rod could be described by

$$u_2(x) = \exp(w\,x)(a_{11}\,\sin(b_1\,x) + a_{12}\,\sin(b_2\,x) + a_{13}\,\cos(b_1\,x) + a_{14}\,\cos(b_2\,x)). \tag{3}$$

The profile by Wang et al. [21] does not include the exponential term because the longitudinal bonding between the wire and the media was neglected to get an analytical solution to the differential equations. In case of a long thin wire embedded in a uniform medium, however, the longitudinal bonding between the wire and the medium is the main reason for the exponentially decaying behavior of the transverse profile [13,19]. Therefore, we have included an exponential term to obtain Eq. (3), which can be used to accurately fit the post-fracture profile.

In addition, since the loading end of the wire does not move transversely, we always have the following boundary condition and thus the relationship between the unknown coefficients:

$$u_2(0) = 0 \Longrightarrow a_{14} = -a_{13}. \tag{4}$$

2.2.1. Forward scheme — energy release rate model

When the lateral displacement is large enough, a crack will nucleate in the vicinity of the first peak of the buckling profile and then propagate into the gelatin medium, both to the left of the peak towards the loading end of the wire, and to the right of the peak, stopping at a distance x_0 from the loading end of the wire. The criteria for crack propagation is: for an increment of crack extension, the amount of strain energy released must be greater than or equal to that required for the surface energy of the two new crack faces. Since gelatin is a soft brittle elastic material, we assume that there is no elastic energy in the fractured gelation zone. Here, x_0 can be considered as the length of the fractured area in which there is no bonding between the wire and the medium, longitudinal or transverse.

Assuming the post-fracture buckling profile of the wire takes the form of $u_2(x)$, we define functions Π_F and S that correspond to the total strain energy of the system after fracture and the energy needed to create a fractured area with the profile $u_2(x)$ from $x = 0$ to $x = x_0$, respectively:

$$\Pi_F = -fv_2(0) + \int_0^L dx \left[\frac{\kappa}{2}u_2''^2(x)\right] + \int_{x_0}^L dx \left[\frac{1}{2}\alpha_\perp u_2^2(x)\right], \tag{5}$$

$$S = 2\gamma \int_0^{x_0} dx|u_2(x)|, \tag{6}$$

where γ is the surface free energy of the gelatin and L is the rod length. In defining Π_F for the post-fracture case, we have ignored the term $\int_{x_0}^L dx[\frac{1}{2}\alpha_\parallel v_2^2(x)]$ as the longitudinal displacement of the wire is negligible in the range of x_0 to L, considering that there is no coupling and thus no longitudinal displacement in the fractured area. In the post-fracture buckling profile defined above in Eq. (3), there are seven unknown coefficients. Since the compressive load is increased quasi-statically in the experiment, if the crack growth speed is slow, then any radiated energy to the surrounding medium during the buckling/fracture process can be neglected in the energy equations. In the post-fracture energy equation Π_F, there is another unknown, which is the crack propagation length x_0. Using the boundary condition at the tip of the wire in Eq. (4), the number of unknowns decreases to seven. To find these seven unknowns using the Griffith crack propagation criteria, we define a new function G:

$$G = \Pi_F + S. \tag{7}$$

When the crack propagation stops, we have $\frac{\partial G}{\partial p_i} = 0$, where p_i is any of the unknown parameters $\{a_{11}, a_{12}, a_{13}, b_1, b_2, w, x_0\}$ that describe the shape of the wire after fracture stops.

Therefore, by taking the partial derivatives of G with respect to the unknowns, seven equations are obtained to satisfy the crack propagation stopping criteria. Considering the conservation of the length of the wire before and after fracture, a Lagrange multiplier is used to incorporate the length equation as the geometrical constraint. So the function that should be minimized is $B = G - m\,\psi$, where $\psi \equiv \int_0^L dx\sqrt{1+u_1{}'(x)^2} - \int_0^L dx\sqrt{1+u_2{}'(x)^2} = 0$ is the length conservation equation, and m is the Lagrange multiplier. Taking the partial derivatives of B with respect to the seven unknowns as well as the Lagrange multiplier, the following set of eight nonlinear equations are obtained and solved simultaneously.

$$\begin{cases} \dfrac{\partial B}{\partial a_{11}} = 0 \\ \dfrac{\partial B}{\partial a_{12}} = 0 \\ \dfrac{\partial B}{\partial a_{13}} = 0 \\ \dfrac{\partial B}{\partial b_1} = 0 \\ \dfrac{\partial B}{\partial b_2} = 0 \\ \dfrac{\partial B}{\partial w} = 0 \\ \dfrac{\partial B}{\partial x_0} = 0 \\ \dfrac{\partial B}{\partial m} = 0. \end{cases} \tag{8}$$

As this is a set of highly nonlinear equations, which has several roots in a wide domain of unknowns, we consider this problem as an optimization problem. It consists of optimizing (minimizing) several objectives simultaneously, with a number of equality constraints. Thus genetic algorithm is used as the optimization method to find the unknowns in a pre-specified domain that is reasonable to the problem at hand. Each one of these eight equations in Eq. (8) is considered to be a single element of a vector in R^8 and then the optimization is run to minimize the Euclidean norm of this vector. The genetic algorithm optimization has been performed separately for all the cases with different gelatin concentrations for a maximum number of generations of 40,000, a population size of 1,000 individuals, an elitism value of 40, a mutation rate of 0.02, and a crossover rate of 0.80.

2.2.2. Backward scheme — energy balancing model

To back up the shape of the buckling profile before fracture in the biopolymer matrix using the post-fracture profile as input, we assume that both the energy of the system and the length of the wire should be unchanged before and after the failure of gelatin, neglecting the friction dissipation during fracture.

Similar to the forward scheme, in this model, we assume that x_0 is the length of the fractured region and $u_2(x)$ in Eq. (3) is the transverse displacement of the thin rod. First, we fit the experimental post-fracture profile to the form of Eq. (3) to find all the six unknowns in the formula. Then we consider the pre-fracture profile to be of the form of Eq. (1). In this model, we have three unknowns, l, u_0 and x_0. The wavelength of the buckling profile before fracture is not treated as an unknown parameter, which can be calculated as a function of the physical properties of the wire and the gelatin. In order to find the three unknown parameters, we use three equations as follows:

$$\int_0^L dx\sqrt{1+u_1{}'(x)^2} = \int_0^L dx\sqrt{1+u_2{}'(x)^2}, \tag{9}$$

$$\int_0^L dx\left[\frac{\kappa}{2}u_1{}''^2(x) + \frac{1}{2}\alpha_\perp u_1^2(x) + \frac{1}{2}\alpha_\parallel v_1^2(x)\right] = \int_0^L dx\left[\frac{\kappa}{2}u_2{}''^2(x)\right] + \int_{x_0}^L dx\left[\frac{1}{2}\alpha_\perp u_2^2(x)\right] + 2\gamma\int_0^{x_0} dx|u_2(x)|, \tag{10}$$

$$\frac{dG}{dx_0} = 0. \tag{11}$$

Eq. (9) is the requirement that the length of the wire remains constant after the failure in the surrounding medium, while Eq. (10) equates the energy of the system before (LHS) and after (RHS) the failure, and Eq. (11) is the crack stopping criteria, where G is defined previously in Eq. (7). The term $2\gamma\int_0^{x_0} dx|u_2(x)|$ in Eq. (10) is associated with the energy required to create two new crack surfaces. We assume that the surrounding medium is intact in the second section ($x \geq x_0$) such that the energy of the system can be computed in the same manner as in the pre-fracture case. It is noteworthy to mention that using L as the upper limit of integrals in Eqs. (9) and (10) instead of the projected length of the wire in the x direction does not affect the results. It is true that the projected length of the buckled wire in the x axis direction is less than the initial wire length. However, as the amplitude of the buckling profile decays exponentially away from the free end of the wire where the compressive loading is exerted, it approaches zero quickly, thus integrating an extra small distance on the distal end of the wire does not affect the energy equations at all.

3. Results and discussion

Using the experimental procedures described in detail in Section 2.1, we are able to find out the buckling profiles of nitinol wires embedded in gelatin with three different concentrations. The wires buckled in a short wavelength form with attenuating amplitude which decayed away from the point where the external force was exerted. As reported in a previous study [13], no-slip coupling assumption up to the moment of fracture is appropriate here, given that the slopes of the force–displacement curves do not change between the buckling initiation points and the catastrophic failure points. If after certain loading a crack is formed along the interface and then propagates only along the interface, there would be an extended stage with a reduced constant slope in the force–displacement curve. Here, although we have not tried to experimentally measure and characterize the crack front, given that in experiments we only observe one constant slope in the force–displacement curve, we know that it must initiate from the interface and then immediately start propagating into the bulk of the surrounding gelatin. This is plausible given that gelatin is, albeit soft, a brittle solid. The rod along with the crack front then continues to propagate into the gelatin, inducing brittle fracture along the way.

Fig. 1(a) shows an example of the buckling profile right before catastrophic fracture happens, when the gelatin concentration is 20 g/l and hinged boundary condition is applied on both ends of the wire. As the buckling profile of the wire is exponentially decaying due to the presence of the gelatin, the lateral displacement of the wire close to the distal end is zero. This means that the presence of an elastic medium effectively enforces the fixed boundary condition at the distal end of the thin rod. Table 1 lists the wavelength λ and the decay length l for the nitinol wire embedded in gelatin right before fracture happened, for the three different concentrations. As the results show the scattering in λ and l is small. These pre-fracture buckling profiles, in the form of $u_1(x)$, were used for input and calibration purposes for our forward and backward schemes.

We also characterized the dynamic buckling shape transition of the wire from the pre-fracture profile to the post-fracture profile, which is shown in a video in the supporting material (S1). This

Table 1
Wavelength and decay length of the pre-fracture buckling profiles for different gelatin concentrations. All sets of mean values and standard deviations are based on testing of three samples.

Gelatin concentrations (g/l)	20	25	30
λ (cm)	6.33 ± 0.21	4.58 ± 0.08	5.24 ± 0.25
l (cm)	3.99 ± 0.39	4.13 ± 0.09	4.85 ± 0.87

whole transition process took roughly 30 s to complete, which renders valid the assumption in the modeling section that the crack growth speed is slow. Interestingly, during this transition, the amplitude of the first wave grows at the expense of the rest of the waves with smaller amplitudes (S1). This is reasonable and the following scenario is deduced. First, as the loading continues, the buckling amplitude increases and the stress/strain increases in the gelatin medium. Then, after reaching the critical strain/stress level at one moment, failure initiates from where the maximum stress/strain is, which is on the rod/medium interface. Once the crack is formed near the peak of the first wave, it can propagate along the wire/gelatin interface, or it can penetrate into the gelatin matrix. As aforementioned, a pure interfacial propagation is impossible. The video indicates that probably both propagation along the interface and penetration into the bulk happen as the crack is pushed to grow by the laterally moving and backward shifting wire. During this process, the energy of longitudinal and transverse bonding in the fractured region is almost completely released because gelatin is a soft and brittle material. For further improvement, one may need to take into account the transverse resistance from the fractured medium, which might be similar to the case of granular medium [16], although this is out of the scope of the current work. The longitudinal and transverse bonding energy in the non-fractured region is also much reduced because of the backward shifting of the wire. Moreover, the bending energy of the wire is reduced through changing from a higher bending mode to a lower bending mode with fewer waves. Fig. 1(b) shows one typical post-fracture profile when the gelatin concentration is 20 g/l.

As previous efforts have shown, the post-fracture profile cannot be fitted using the pre-fracture exponentially decaying profile [22]. We have also tried more complicated formula such as an exponentially decaying term multiplied by summation of two sine terms. However, they cannot fit the post-fracture profile reasonably well. Inspired by the recent work by Wang et al. [21], we adopted the form in Eq. (3) in Section 2.2. As Fig. 1(c) and (d) show, adopting these ansatzs for the pre-fracture and post-fracture profiles, we can get perfect fitting to the experimentally captured buckling profiles.

For the calculation of the potential energy in the theory and modeling work, the shear moduli of the gelatin are estimated using Fig. 2(a) in Ref. [19] to be 0.64 kPa, 0.87 kPa and 1.12 kPa for concentrations of 20 g/l, 25 g/l and 30 g/l, respectively. Surface energies of gelatins are interpolated based on data in Ref. [23] to be 0.80 J/m^2, 0.86 J/m^2, and 0.93 J/m^2 for the gelatin with concentrations of 20 g/l, 25 g/l, and 30 g/l, respectively. Note that, since the buckling profiles are magnified by the graduated cylinder filled with gelatin by a scaling factor of $\sim$1.1, in the calculation of all the energy terms, the real buckling profiles are backed up first and then used. This is the case for both the pre-fracture profiles and the post-fracture profiles. For both forward and backward schemes, the pre-specified domain for the length of the fractured region, x_0, in the genetic algorithm optimization method is set to be from 0.015 m to 0.10 m. This covers the area with nonzero transverse displacement in the post-fracture buckling profiles obtained from experiments, starting roughly from the first peak of the pre-fractured buckling profiles, as shown in Fig. 1.

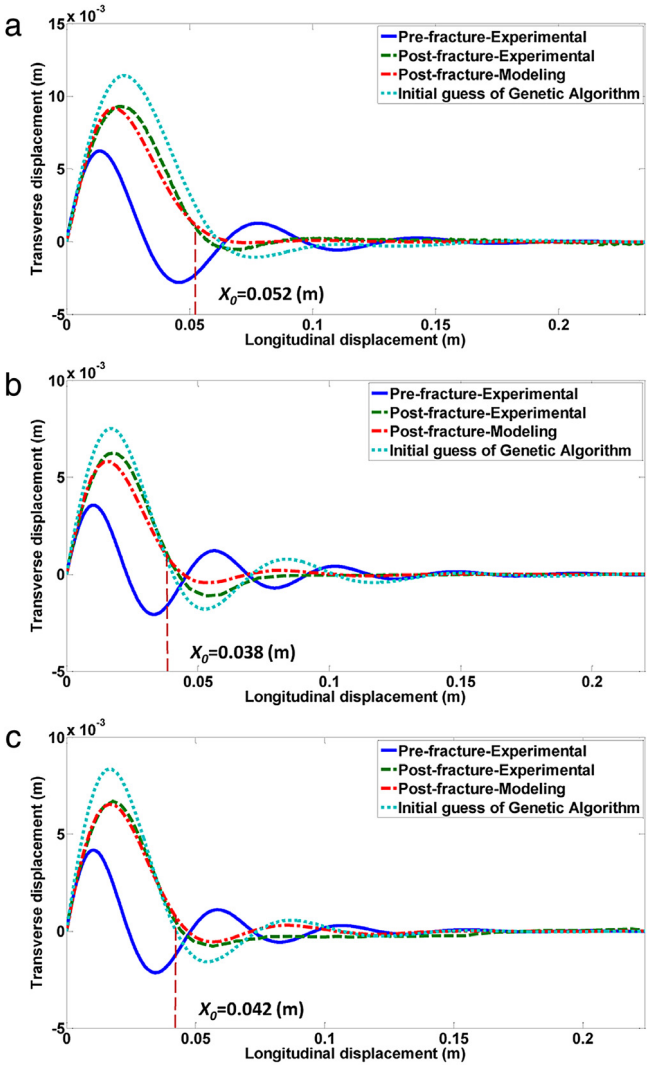

Fig. 3. Post-fracture buckling profiles predicted from the forward scheme for three gelatin concentrations with position of x_0 marked: (a) 20 g/l (b) 25 g/l (c) 30 g/l.

Using the forward scheme described earlier in Section 2.2.1, we solved the system of nonlinear equations to predict the wire buckling profile after the medium failure using genetic algorithm. Fig. 3 shows the results obtained from the forward scheme for three gelatin concentrations listed in Table 1. Note that we randomly picked one profile among the three experimentally obtained since the variation across them is small and we cannot work on the average values listed in Table 1. We did this for all three concentrations. As can be seen, the constrained optimization model solved by genetic algorithm can predict the post-fracture buckling profile reasonably well; the initial guess for the genetic algorithm does not affect the final results as it should not. This model can capture the amplitude and the wavelength of the post-fracture profile in a reasonably good agreement with the experimental data; however it cannot accurately capture the overshoot of the profile after the first peak. We also tried different values of surface energy of the surrounding gelatin to investigate its effect on the final results and found out that it is not significant in the estimated range [23].

Fig. 4 shows the results of the backward scheme described in Section 2.2.2. Same as for the forward scheme, we randomly picked one profile among the available three for all concentrations. It is shown that this model can perfectly capture the amplitude and the decay length of the transverse buckling profile of the wire.

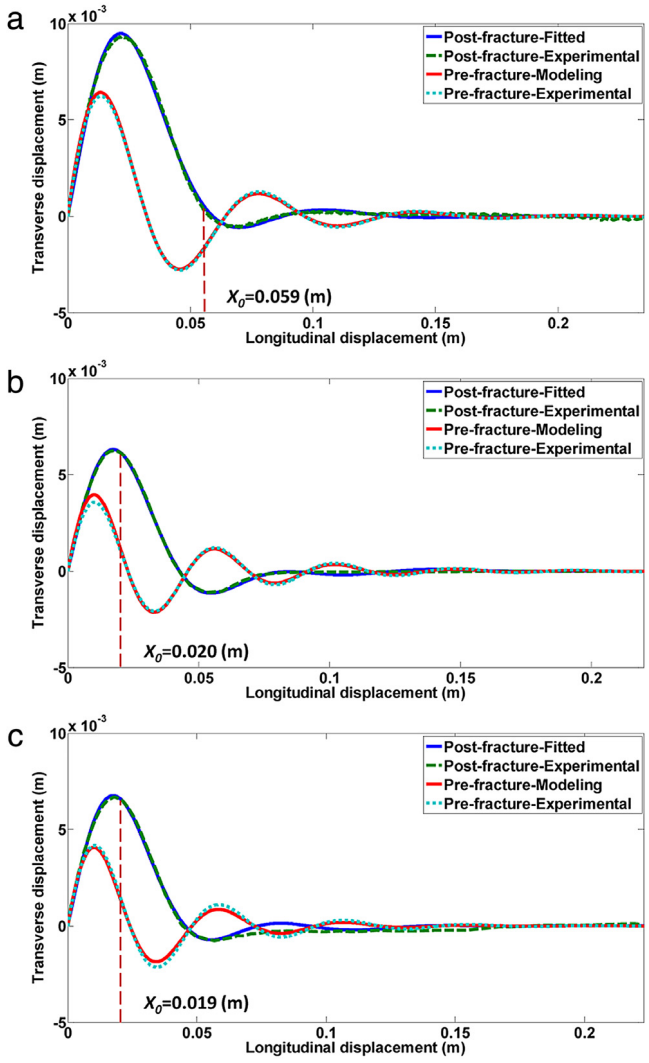

Fig. 4. Pre-fracture buckling profiles backed up from the backward scheme for three gelatin concentrations with position of x_0 marked: (a) 20 g/l (b) 25 g/l (c) 30 g/l.

This scheme takes much less time to converge when compared to the forward scheme because the more complicated post-fracture profile is given as the input, instead of the target to predict in the forward scheme. The number of unknowns is three in contrast with eight for the forward scheme. As shown by Figs. 3 and 4, the backward scheme generates better estimations as the task is less challenging.

It is worthwhile to point out that the values of x_0 predicted from the forward and backward schemes are in the interval of (0.042 m, 0.052 m) and (0.019 m, 0.059 m), respectively. The minor difference might be caused by the different models we adopted for the forward and backward schemes. That is, energy release rate for crack stopping criteria in the forward scheme, whereas energy balance in the backward scheme. Nonetheless, both schemes are able to predict the buckling profiles reasonably well and the values of x_0 remain reasonably consistent. As our understanding of these phenomena develops further, more interesting findings may unfold, which could help interpret the mechanics of thin wire buckling ubiquitously found in nature.

4. Conclusions

We have conducted a combination of experimental and computational investigations into the buckling shape transition of a thin wire embedded in a fractured elastic medium. We experimentally characterized the dynamic transition and identified the appropriate function form to quantify the post-fracture buckling profile. We presented a forward scheme and a backward scheme to predict and back up the buckling shapes of the thin elastic wire before and after the surrounding medium fails. Taking the pre-fracture buckling profile as input, we used Griffith's crack propagation stopping criteria in the forward scheme to predict the post-fracture buckling profile of the wire; results show that this model can predict the shape of the post-fracture profile in a reasonably good agreement with the experimental data. Furthermore, taking the post-fracture buckling profile as input, we balanced the energy of the system before and after fracture in the backward scheme to back up the pre-fracture buckling profile, which resulted in an almost perfect agreement with the experimental data. The methodologies developed here can be generalized to describe the mechanical behavior of other systems containing a thin elastic rod embedded in a soft brittle elastic gel. They also set as the first effort ever to investigate the rich yet poorly understood mechanics of reinforced buckling of thin elastic rods when large deformations such as failure are present.

Acknowledgements

A.M. and W.S. acknowledge the support from the University of Nevada, Reno startup fund. Z.C. acknowledges the support from the Dartmouth College startup fund and the Society in Science - Branco Weiss fellowship, administered by ETH Zürich.

References

[1] A.R. Dexter, J.S. Hewitt, J. Agric. Eng. Res. 23 (1978) 17–22.
[2] J.L. Silverberg, R.D. Noar, M.S. Packer, M.J. Harisson, C.L. Henley, I. Cohen, S.J. Gerbode, Proc. Natl. Acad. Sci. USA 109 (42) (2012) 16794–16799.
[3] K. Arjomandi, F. Taheri, Int. J. Press. Vessels Pip. 88 (4) (2011) 138–148.
[4] A.J. Neto, C.A. Martins, J. Offshore Mech. Arct. Eng. 134 (2012) 031701.
[5] D.K. Xing, J.M. Zheng, J. Chem. Pharm. Res. 5 (9) (2013) 182–187.
[6] K. Pan, Y. Ni, L. He, R. Huang, Int. J. Solids Struct. 51 (2014) 3715–3726.
[7] A. Khamlichi, M. Bezzazi, A. Limam, Thin-Walled Struct. 42 (2004) 1035–1047.
[8] C. Androulidakis, E.N. Koukaras, O. Frank, G. Tsoukleri, D. Sfyris, J. Parthenios, C. Galiotis, Sci. Rep. 4 (2014) 5271.
[9] C.P. Brangwynne, F.C. MacKintosh, S. Kumar, L. Mahadevan, N. Geisse, K.K. Parker, D.E. Ingber, D.A. Weitz, J. Cell Biol. 173 (2006) 733–741.
[10] M. Das, A.J. Levine, F.C. MacKintosh, Europhys. Lett. 84 (2008) 18003.
[11] T. Li, J. Biomech. 41 (2008) 1722–1729.
[12] H. Jiang, J. Zhang, J. Appl. Mech. 75 (2008) 061019.
[13] W.L. Shan, Z. Chen, C.P. Broedersz, A.A. Gumaste, W.O. Soboyejo, C.P. Brangwynne, Soft Matter 9 (2013) 194–199.
[14] T. Su, J. Liu, D. Terwagne, P.M. Reis, K. Bertoldi, Soft Matter 10 (2014) 6294–6302.
[15] S.G. O'Keeffe, D.E. Moulton, S.L. Waters, A. Goriely, Int. J. Non-Linear Mech. 56 (2013) 94–104.
[16] A.R. Mojdehi, B. Tavakol, W. Royston, D.A. Dillard, D.P. Holmes, Extreme Mech. Lett. 9 (1) (2016) 237–244.
[17] Y. Xiao, D. Hayman, S.S. Khalafvand, M.L. Lindsey, H.C. Han, Am. J. Physiol. Heart Circ. Physiol. 307 (2014) H542–H551.
[18] D. Hui, Int. J. Non-Linear Mech. 23 (2) (1988) 113–123.
[19] A. Bot, I.A.V. Amerongen, R.D. Groot, N.L. Hoekstra, W.G.M. Agterof, Polym. Gels Netw. 4 (1996) 189–227.
[20] X. Wang, W. Hong, Soft Matter 8 (2012) 8171–8178.
[21] D. Wang, S. Huang, N. Hu, A. Mohammadi Nasab, H. Grover, M.C. Abate, L. Tan, X. Yu, W.L. Shan, Z. Chen, 2017 (In preparation).
[22] A. Mohammadi Nasab, Z. Chen, W.L. Shan, J. Postdr. Res. 3 (6) (2015) 1–4.
[23] J.L. Kavanagh, T. Men, K.A. Daniels, Tectonophysics 582 (2013) 101–111.